Fibronectin Adsorption onto Polyelectrolyte Multilayer Films

A. Pascal Ngankam,[†] Guangzhao Mao,[‡] and Paul R. Van Tassel*,[†]

Department of Chemical Engineering, Yale University, P.O. Box 208286, New Haven, Connecticut 06520, and Department of Chemical Engineering and Materials Science, Wayne State University, Detroit, Michigan 48202

Received August 12, 2003. In Final Form: December 19, 2003

The Layer-by-layer deposition of positively and negatively charged macromolecular species is an ideal method for constructing thin films incorporating biological molecules. We investigate the adsorption of fibronectin onto polyelectrolyte multilayer (PEM) films using optical waveguide lightmode spectroscopy (OWLS) and atomic force microscopy (AFM). PEM films are formed by adsorption onto $Si(Ti)O_2$ from alternately introduced flowing solutions of anionic poly(sodium 4-styrenesulfonate) (PSS) and cationic poly(allylamine hydrochloride) (PAH). Using OWLS, we find the initial rate and overall extent of fibronectin adsorption to be greatest on PEM films terminated with a PAH layer. The polarizability density of the adsorbed protein layer, as measured by its refractive index, is virtually identical on both PAH- and PSS-terminated films; the higher adsorbed density on the PAH-terminated film is due to an adsorbed layer of roughly twice the thickness. The binding of monoclonal antibodies specific to the protein's cell binding site is considerably enhanced to fibronectin adsorbed to the PSS layer, indicating a more accessible adsorbed layer. With increased salt concentration, we find thicker PEM films but considerably thinner adsorbed fibronectin layers, owing to increased electrostatic screening. Using AFM, we find adsorbed fibronectin layers to contain clusters; these are more numerous and symmetric on the PSS-terminated film. By considering the electrostatic binding of a segmental model fibronectin molecule, we propose a picture of fibronectin adsorbed primarily in an end-on-oriented monolayer on a PAH-terminated film and as clusters plus side-on-oriented isolated molecules onto a PSS-terminated film.

Introduction

The placement of biological or biomimetic structure onto or within synthetic materials portends significant advances in biosensing surfaces, drug delivery vehicles, and tissue engineering substrates. Physical adsorption of biomolecules from solution is a simple and elegant method but with only limited control over adsorbed layer structure. Binding to surface-immobilized, high-affinity ligands offers a greater degree of translational and orientational order but requires extensive surface functionalization. A simpler means of controlling the structure of physisorbed biomolecular layers is through a thin film coating made via, for example, the Langmuir−Blodgett (LB)[1] or the Layer-by-layer (LbL)[2] method.

Of these, the LbL method is particularly promising for producing thin films of controlled structure and chemical architecture for a variety of applications, including biocompatible synthetic substrates. In LbL, a film is grown by alternately exposing a substrate to solutions of positively and negatively charged adsorbing species. So long as each exposure results in charge overcompensation, the process may continue over many layers. Unlike their LB counterparts, LbL films are away from equilibrium and, thus, are influenced by processing condition variables that are generally more numerous than the relevant thermodynamic degrees of freedom. Polyelectrolyte multilayer (PEM) films, in which the charged species are cationic and anionic polymers, are an important subclass of LbL materials. In particular, proteins embedded in or adsorbed onto PEM films are potentially useful in tissue engineering and drug delivery.[3] Several reports of this have appeared recently.[4−32] Of particular significance have been studies showing proteins adsorbed on or embedded

* To whom correspondence should be addressed. Phone: 203-432-7983. Fax: 203-432-4387. E-mail: paul.vantassel@yale.edu.
[†] Yale University.
[‡] Wayne State University.

(1) Roberts, G., Ed. *Langmuir−Blodgett Films*; Plenum Press: New York, 1990.
(2) Decher, G.; Schlenoff, J. B., Eds. *Multilayer Thin Films*; Wiley-VCH: Weinheim, 2003.
(3) Jessel, N.; Atalar, F.; Lavalle, P.; Mutterer, J.; Decher, G.; Schaaf, P.; Voegel, J. C.; Ogier, J. *Adv. Mater.* **2003**, *15*, 692−695.
(4) Lvov, Y.; Ariga, K.; Kunitake, T. *Chem. Lett.* **1994**, 2323−2326.
(5) Lvov, Y.; Ariga, K.; Ichinose, I.; Kunitake, T. *J. Am. Chem. Soc.* **1995**, *117*, 6117−6123.
(6) Lvov, Y.; Ariga, K.; Ichinose, I.; Kunitake, T. *Thin Solid Films* **1996**, *285*, 797−801.
(7) Onda, M.; Lvov, Y.; Ariga, K.; Kunitake, T. *Biotechnol. Bioeng.* **1996**, *51*, 163−167.
(8) Caruso, F.; Niikura, K.; Furlong, D. N.; Okahata, Y. *Langmuir* **1997**, *13*, 3427−3433.
(9) Caruso, F.; Furlong, D. N.; Ariga, K.; Ichinose, I.; Kunitake, T. *Langmuir* **1998**, *14*, 4559−4565.
(10) Cassier, T.; Lowack, K.; Decher, G. *Supramol. Sci.* **1998**, *5*, 309−315.
(11) He, J. A.; Samuelson, L.; Li, L.; Kumar, J.; Tripathy, S. K. *J. Phys. Chem. B* **1998**, *102*, 7067−7072.
(12) Caruso, F.; Mohwald, H. *J. Am. Chem. Soc.* **1999**, *121*, 6039−6046.
(13) Caruso, F.; Schuler, C. *Langmuir* **2000**, *16*, 9595−9603.
(14) Caruso, F.; Fiedler, H.; Haage, K. *Colloids Surf., A* **2000**, *169*, 287−293.
(15) Ladam, G.; Gergely, C.; Senger, B.; Decher, G.; Voegel, J. C.; Schaaf, P.; Cuisinier, F. J. G. *Biomacromolecules* **2000**, *1*, 674−687.
(16) Li, M. L.; Li, B. F.; Jiang, L.; Tussila, T.; Tkachenko, N.; Lemmetyinen, H. *Sci. China, Ser. B* **2000**, *43*, 313−322.
(17) Schuler, C.; Caruso, F. *Macromol. Rapid Commun.* **2000**, *21*, 750−753.
(18) Ladam, G.; Schaaf, P.; Cuisinier, F. J. G.; Decher, G.; Voegel, J. C. *Langmuir* **2001**, *17*, 878−882.
(19) Balabushevitch, N. G.; Sukhorukov, G. B.; Moroz, N. A.; Volodkin, D. V.; Larionova, N. I.; Donath, E.; Mohwald, H. *Biotechnol. Bioeng.* **2001**, *76*, 207−213.
(20) Muller, M.; Rieser, T.; Dubin, P. L.; Lunkwitz, K. *Macromol. Rapid Commun.* **2001**, *22*, 390−395.
(21) Ram, M. K.; Bertoncello, P.; Ding, H.; Paddeu, S.; Nicolini, C. *Biosens. Bioelectron.* **2001**, *16*, 849−856.
(22) Santos, J. P.; Welsh, E. R.; Gaber, B. P.; Singh, A. *Langmuir* **2001**, *17*, 5361−5367.

10.1021/la035479y CCC: $27.50
Published on Web 03/19/2004

in PEM films to retain at least part of their biological activity,[8] suggesting the interactions responsible for conformation (hydrogen bonding, hydration forces, electrostatic interactions) are not too greatly perturbed by the PEM film. Although several energetic factors influence macromolecules on PEM films, Ladam et al.[18] recently presented convincing evidence showing electrostatic interactions to be dominant. From a physicochemical point of view, proteins are polyampholytes bearing patches of positively and negatively charged zones on their surfaces. One of our objectives is to exploit the interactions of these patches with an underlying PEM film to control protein orientation.

Fibronectin (FN) is a highly flexible glycoprotein composed of functionally specific domains.[33−35] It plays an important role in numerous biological phenomena including cell adhesion and spreading, wound healing, phagocytosis, and differentiation. FN communicates with living cells through contact between its cell binding site (containing the Arg-Gly-Asp amino acid sequence) and integrin proteins located within the cell's membrane. Materials coated with FN are natural choices for tissue engineering substrates. However, the optimal manner in which the protein is to be presented to a cell remains an open question. Ideal might be protein layers oriented in a way that maximizes exposure of the cell binding site and minimizes alteration of its internal conformation. Indeed, the biological activity of FN is known to be sensitive to conformation.[36−39] PEM films, whose surface charge and topography may be controlled through the LbL fabrication process, offer the possibility to bind FN at an optimal orientation while preserving (and perhaps stabilizing) its internal conformation.

Even on simple surfaces, a degree of structural control may be exerted on FN layers by altering the deposition conditions. Guemouri et al. found FN to exist in a compact conformation prone to lateral clustering following adsorption from a low-ionic-strength solution and adsorption from a high-ionic-strength solution to lead to a random extended conformation.[40] Owing to the greater structural variability in a PEM film compared to a simple surface, one expects an even greater degree of control over the adsorbed protein layer.

In this paper, we investigate the adsorption of FN onto a PEM film composed of poly(allylamine hydrochloride) (PAH) and poly(sodium 4-styrenesulfonate) (PSS). We employ optical waveguide lightmode spectroscopy (OWLS) to continuously measure the refractive index, thickness, and density of the PEM film and protein adlayer and atomic force microscopy (AFM) to measure the topographical structure of the PEM films with and without a FN layer. The two methods are highly complementary: the former provides exquisite sensitivity to the kinetics but provides only average film properties, while the latter allows for a determination of lateral structural heterogeneities on the nanometer scale, albeit at a lower time resolution. Our objective is to determine the influence of the PEM film composition and formation conditions on the structure and formation kinetics of a subsequently placed FN layer.

Experimental Section

Protein, Polyelectrolyte, and Buffer. Human plasma fibronectin[34] (FN, MW ca. 550 kD, pI 5.5−6.3, 0.1% solution in 0.05 M Tris buffered saline at pH 7.5), cationic PAH (MW ca. 70 000, chemical formula $[-CH_2CH(CH_2NH_2{\cdot}HCl)-]_n$), and anionic PSS (MW ca. 70 000, chemical formula $[-CH_2CH(C_6H_4(NaSO_3))-]_n$) are obtained from the Aldrich Chemical Co. Mouse monoclonal IgG_1 (AntiFN, MW ca. 150 kD, pI ca. 8.0, in 1.0 mL of phosphate buffered saline containing 0.1% sodium azide and 2% gelatin) is obtained from Santa Cruz Biotechnology, Inc. All chemicals are used without further purification and are dissolved in a filtered (Millipore, 0.4 μm) HEPES buffer made from 10 mM *N*-(2-hydroxyethyl)piperazine-*N*′-2-ethanesulfonic acid (obtained from Sigma Chemical), 100 mM NaCl (obtained from Fluka), and deionized water (of conductivity 1.30 ± 0.05 μS and pH 5.5−6). The final pH of the buffer is adjusted to 7.4 by adding a few drops of 6 N NaOH. The prepared buffer solution is degassed in an ultrasonic bath for 30 min prior to use.

Adsorbing Surface. Our adsorbing surface is a planar silicon titanium oxide (STO) waveguide of chemical composition $Si_{1-x}Ti_xO_2$ ($x = 0.25 \pm 0.05$). The waveguiding film is part of an OW 2400 sensor chip (MicroVacuum, Budapest) consisting of a glass support (of thickness ca. 1.5 mm and refractive index ca. 1.55) and the waveguiding film (of thickness ca. 200 nm and refractive index ca. 1.77) with an embossed diffraction grating (of 2400 lines/mm) across its center. The waveguide serves as the bottom to our flow cell of volume 70 μL.

Prior to each experiment, the flow cell and tubing are cleaned with a 2% Hellmanex (Hellma, Mulheim, Germany) solution in ultrapure water for 2 h. The sensor chip is cleaned in this same solution in an ultrasonic bath. Special care must be taken not to destroy the STO coating by a long time exposure to the Hellmanex solution. The cleaned sensor chips are used for both the OWLS and the AFM experiments.

OWLS Experiments. OWLS is an evanescent wave technique based on integrated optics[41] used to investigate the adsorption of protein, polymers, and "small" spherical particles at the solid (waveguide)/liquid interface.[42,43] The basic OWLS sensing principles are described elsewhere in detail.[44,45] Here, OWLS is used to continuously measure the formation of a PEM film on a STO surface and the subsequent adsorption of FN to this film. In certain experiments, monoclonal IgG binding to the FN/PEM film is also measured to test binding site accessibility.

A sensor chip (see previous text) previously soaked overnight in HEPES buffer solution is mounted to a cylindrical aluminum flow cell of volume 70 μL. The flow cell/sensor chip assembly is

(23) Schwinte, P.; Voegel, J. C.; Picart, C.; Haikel, Y.; Schaaf, P.; Szalontai, B. *J. Phys. Chem. B* **2001**, *105*, 11906−11916.
(24) Yang, W. J.; Trau, D.; Renneberg, R.; Yu, N. T.; Caruso, F. *J. Colloid Interface Sci.* **2001**, *234*, 356−362.
(25) Hoshi, T.; Akase, S.; Anzai, J. *Langmuir* **2002**, *18*, 7024−7028.
(26) Jussila, T.; Li, M. L.; Tkachenko, N. V.; Parkkinen, S.; Li, B. F.; Jiang, L.; Lemmetyinen, H. *Biosens. Bioelectron.* **2002**, *17*, 509−515.
(27) Ladam, G.; Schaaf, P.; Decher, G.; Voegel, J. C.; Cuisinier, F. J. G. *Biomol. Eng.* **2002**, *19*, 273−280.
(28) Meier-Haack, J.; Muller, M. *Macromol. Symp.* **2002**, *188*, 91−103.
(29) Richert, L.; Lavalle, P.; Vautier, D.; Senger, B.; Stoltz, J. F.; Schaaf, P.; Voegel, J. C.; Picart, C. *Biomacromolecules* **2002**, *3*, 1170−1178.
(30) Schwinte, P.; Ball, V.; Szalontai, B.; Haikel, Y.; Voegel, J. C.; Schaaf, P. *Biomacromolecules* **2002**, *3*, 1135−1143.
(31) Simonian, A. L.; Revzin, A.; Wild, J. R.; Elkind, J.; Pishko, M. V. *Anal. Chim. Acta* **2002**, *466*, 201−212.
(32) Tiourina, O. P.; Sukhorukov, G. B. *Int. J. Pharm.* **2002**, *242*, 155−161.
(33) Mosher, D. F., Ed. *Fibronectin. Biology of the Extracellular Matrix: A Series*; Academic Press: San Diego, 1989.
(34) Hynes, R. O. *Fibronectins*; Springer-Verlag: New York, 1990.
(35) Potts, J. R.; Campbell, I. D. *Matrix Biol.* **1996**, *15*, 313−320.
(36) Williams, E. C.; Janmey, P. A.; Ferry, J. D.; Mosher, D. F. *J. Biol. Chem.* **1982**, *257*, 4973−4978.
(37) Lewandowska, K.; Pergament, E.; Sukenik, C. N.; Culp, L. A. *J. Biomed. Mater. Res.* **1992**, *26*, 1343−1363.
(38) Underwood, P. A.; Steele, J. G.; Dalton, B. A. *J. Cell Sci.* **1993**, *104*, 793−803.
(39) Ugarova, T. P.; Zamarron, C.; Veklich, Y.; Bowditch, R. D.; Ginsberg, M. H.; Weisel, J. W.; Plow, E. F. *Biochemistry* **1995**, *34*, 4457−4466.
(40) Guemouri, L.; Ogier, J.; Zekhnini, Z.; Ramsden, J. J. *J. Chem. Phys.* **2000**, *113*, 8183−8186.
(41) Tien, P. K. *Rev. Mod. Phys.* **1977**, *49*, 361−420.
(42) Ramsden, J. J. *Chimia* **1999**, *53*, 67−71.
(43) Voros, J.; Ramsden, J. J.; Csucs, G.; Szendro, I.; De Paul, S. M.; Textor, M.; Spencer, N. D. *Biomaterials* **2002**, *23*, 3699−3710.
(44) Tiefenthaler, K.; Lukosz, W. *J. Opt. Soc. Am. B* **1989**, *6*, 209−220.
(45) Ramsden, J. J. *J. Stat. Phys.* **1993**, *73*, 853−877.

inserted into the head of a precision goniometer that is part of a BIOS-1 OWLS instrument (MicroVacuum, Budapest). HEPES buffer is then introduced into the flow cell by a peristaltic pump at a constant shear rate at the adsorbing surface of $1.3 \pm 0.3\ s^{-1}$. This shear rate is also used during all subsequent adsorption experiments. A HeNe laser beam (of wavelength $\lambda = 632.8$ nm) is then directed toward the sensor chip while the goniometer rotates. A guided mode of effective refractive index N is excited when the incoupling condition $N = n_{air} \sin \alpha + (l\lambda/\Lambda)$ is satisfied, where n_{air} is the refractive index in air, α is the angle between the laser and the waveguide, l is the diffraction order, and Λ is the grating line spacing. Effective refractive indices associated with the zeroth transverse electric and transverse magnetic modes (N_{TE} and N_{TM}) are measured, and once steady values are achieved, a polyelectrolyte solution is added.

PEM films are built by alternately introducing flowing solutions of PAH and PSS dissolved in HEPES ($c_{PAH} = c_{PSS} = 5$ μg/mL) into the flow cell for a period of 7 min; these are separated by 7-min HEPES buffer rinses. An exception is the initial layer, which is introduced for a period of 10 min to allow the kinetic curve to reach a plateau. During PEM film formation, values of N_{TE} and N_{TM} are determined every 22.9 s and are used to calculate the thickness and refractive index of the (assumed optically uniform) PEM film via[44]

$$2\pi m = \frac{2\pi}{\lambda}(n_F^2 - N^2)^{1/2} t_F + t_A \frac{n_A^2 - n_C^2}{n_F^2 - n_C^2}\left[\frac{(N/n_C)^2 + (N/n_A)^2 - 1}{(N/n_C)^2 + (N/n_F)^2 - 1}\right]^{\rho} - \arctan\left(\frac{n_F}{n_S}\right)^{2\rho}\left(\frac{N^2 - n_S^2}{n_F^2 - N^2}\right)^{1/2} - \arctan\left(\frac{n_F}{n_C}\right)^{2\rho}\left(\frac{N^2 - n_C^2}{n_F^2 - N^2}\right)^{1/2} \quad (1)$$

where n and t are the refractive index and thickness of the waveguiding film (F), adlayer (A), or cover solution (C), m is the mode number ($m = 0$ for the waveguides used here), and $\rho = 0$ and 1 for TE and TM modes, respectively. n_F and d_F are determined from eq 1, with d_A set to 0, during the initial buffer exposure, and n_C is determined using a refractometer (AR 600, Leica Microsystems, Buffalo). The adlayer's density (Γ) may then be calculated using de Feijter et al.'s formula:[46]

$$\Gamma = d_A(n_A - n_C)\left(\frac{dn}{dc}\right)^{-1} \quad (2)$$

where dn/dc is the change in the refractive index with bulk concentration, which for PAH−PSS films is taken to be 0.197 mL/mg.[47] Films composed of (i) four PAH−PSS bilayers with an additional PAH terminal layer and (ii) five PAH−PSS bilayers are built. These are referred to here as $(PAH-PSS)_4-PAH$ and $(PAH-PSS)_5$, respectively.

Once the PEM film is established, a solution of FN in HEPES is introduced and the effective refractive indixes are again measured. The thickness and refractive index of the (assumed optically uniform) FN−PEM layer are calculated from eq 1, and from these, the protein density is determined via eq 2 with $dn/dc = 0.182$.[46] [Analyses of OWLS data for the PEM−protein film in terms of (i) a single optically uniform layer and (ii) two optically uniform layers, one each representing the PEM and the protein layers, yield little difference in the measured thickness or density.][48] Measurements continue until a semiplateau is reached, defined as the point where the differences between 10 consecutive measured values of N_{TE} are less than 5×10^{-6}. A buffer rinse follows. All experiments for FN concentrations of 50 μg/mL are repeated using a high-ionic-strength HEPES buffer ([NaCl] = 1.0 M).

Finally, following certain experiments, a solution of monoclonal IgG (AntiFN) in HEPES buffer at a concentration of 0.5 μg/mL is introduced. This antibody binds specifically to the cell binding site of FN, which is located near to the molecule's center.[35] The purpose of this step is to probe the accessibility of this site and, thereby, the orientation and conformation of the adsorbed FN. As a control, in certain other experiments, a solution of monoclonal IgG specific to a different protein, cytochrome c (AntiCC), is introduced in an otherwise identical way.

AFM Experiments. AFM is used to obtain morphological information and the relative thicknesses of either the PEM film or the FN + PEM film. AFM samples are prepared with the OWLS flow cell attached to a 15-mm-diameter disk cut from a new sensor chip. The film growth procedure is identical to that described previously, except that, because of the required cutting of the sensor chip (to allow insertion into the AFM instrument), no OWLS signal is recorded during the sample preparation.

All AFM images are captured by a Nanoscope III (Digital Instruments, Inc.) in contact mode with scanner E. The z scale of the scanner is calibrated with the Ultra-Sharp Calibration TGZ02 set (step height 100 nm, Silicon-MDT). Silicon nitride (Si_3N_4) integral tips (NP type) are used with a nominal tip radius of 20−40 nm. Height images are captured with feedback gains between 3 and 5 and are flattened to remove background slopes. No other filtering procedures are performed on these images. Each sample is scanned at several randomly chosen locations to investigate homogeneity. For a given sample, differences between locations are negligible.

Results

PEM Film Formation. In Figure 1, we show the optical thickness (t_A), refractive index (n_A), and density (Γ) of the PEM film versus time as calculated from eqs 1 and 2. The upward arrows represent the introduction of either a PAH or PSS solution, and the downward arrows represent the introduction of a pure buffer solution. (We note that eq 1 is not solvable for films composed of fewer than three layers, probably as a result of their small thickness and their nonuniform nature.) PSS layer growth appears to be very standard. During exposure to the PSS solution, the film density and refractive index increase steadily to a virtual plateau and the thickness increases abruptly to a sharp plateau. During a buffer rinse, a modest desorption occurs resulting in a thinner but more optically dense layer. In contrast, PAH layer growth is somewhat unusual. During exposure to the PAH solution, the film thickness (refractive index) increases (decreases) considerably. This effect is most pronounced for the initial layers. The film density reaches an abrupt plateau following an initial increase. During a buffer rinse, the thickness (refractive index) shows a significant decrease (increase) and the density decreases initially but shows a slight asymptotic increase (this latter feature is clearly an artifact). We propose a picture where the layer grows initially by an irreversible adsorption of PAH in a flat conformation and then continues to grow by reversible adsorption in a much more extended conformation. These extended chains contribute greatly to the film thickness and cause the overall refractive index to be low. They do not contribute greatly to the overall density and are removed during a buffer rinse. We depict our hypothesis in Figure 2.

During the LbL construction of the PEM film, beginning with the third layer, we observe the thickness and the adsorbed density of the PEM film to increase linearly with the number of adsorbed polyelectrolyte layers whereas the refractive index remains nearly constant. The incremental thickness of a PAH−PSS bilayer was 3.1 ± 0.1 nm, which is somewhat smaller than the 5.3 ± 0.2 nm found by Picart et al.[48] in Tris buffers (pH 7.35) of [NaCl] = 0.15 M. This discrepancy may be due to the difference in the surface charge between STO and silica or to their use of an initial adsorbed layer of high-density polyethylene imine as a PEM precursor. In any event, our value

(46) de Feijter, J. A.; Bejamins, J.; Veer, F. A. *Biopolymers* **1978**, *17*, 1759.

(47) Ladam, G.; Schaad, P.; Voegel, J. C.; Schaaf, P.; Decher, G.; Cuisinier, F. *Langmuir* **2000**, *16*, 1249−1255.

(48) Picart, C.; Ladam, G.; Senger, B.; Voegel, J. C.; Schaaf, P.; Cuisinier, F. J. G.; Gergely, C. *J. Chem. Phys.* **2001**, *115*, 1086−1094.

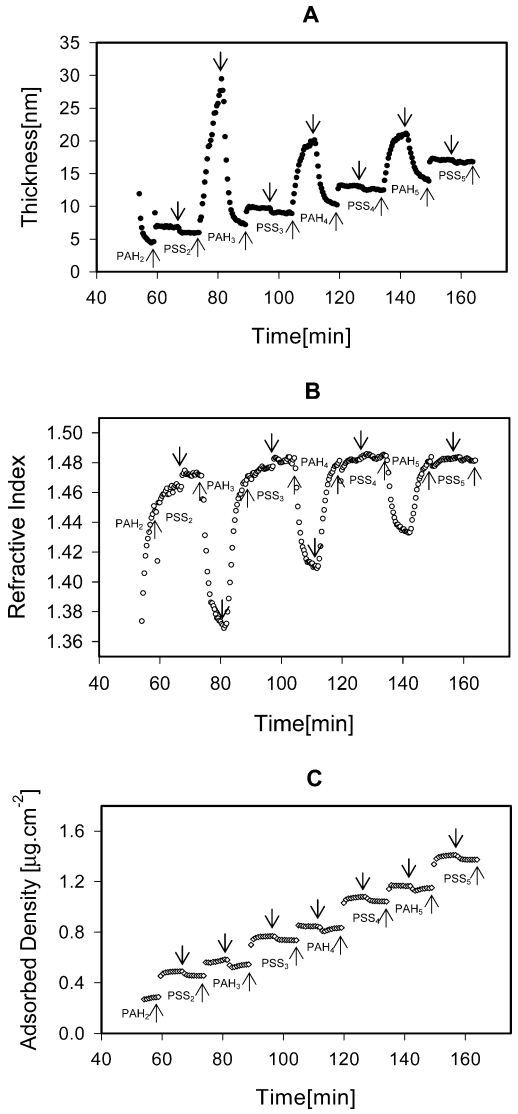

Figure 1. (A) Optical thickness, (B) refractive index, and (C) adsorbed density versus time as determined via OWLS. The upward arrows represent the introduction of either PAH or PSS solutions, of concentration 5 μg/mL in HEPES buffer of [NaCl] = 0.1 M, into the flow cell, and the downward arrows represent the introduction of pure buffer. The adsorption and buffer rinse times during the formation of the first layer are 10 min and those of subsequent layers are 7 min.

is certainly of an expected magnitude. (We note that Ramsden et al. measured the PAH−PSS bilayer thickness on STO during a water rinse, where significant swelling is expected, to be 7.8 nm.)[49,50] Additionally, we note the refractive index of PEM films $(PAH-PSS)_n-PAH$ ($2 \leq n \leq 4$) to be consistently lower than those of films $(PAH-PSS)_n$ or $(PAH-PSS)_{n+1}$; this is likely related to the unusual PAH growth behavior mentioned previously. The parameters of PEM films used subsequently for FN adsorption appear in Table 1. The values shown are averages over three identical experiments. Uncertainties represent the standard deviation among the three runs.

FN Adsorption. In Figure 3A, we show the adsorption kinetics of FN from a solution of concentration 50 μg/mL onto $(PAH-PSS)_4-PAH$ (positively charged) and $(PAH-PSS)_5$ (negatively charged) PEM films. The arrows show the onset of a buffer rinse. We observe the overall extent of adsorption to greatly differ; the plateau on the positively charged, PAH terminating layer is almost double that of the one on the negatively charged, PSS terminating layer. The weak decrease of the adsorbed FN density on both PEM films during the buffer rinse testifies to the strength of the attachment. We show the discrete time derivative of these kinetics curves in Figure 3b. Both systems exhibit an initial transient transport-limited regime, characterized by an increasing rate of adsorption, followed by a surface-limited regime. The crossover between these two regimes occurs at a higher density (and longer time) for the $(PAH-PSS)_4-PAH$ film, indicating more rapid adsorption to the film. We further analyze these rate curves in the Discussion section to follow.

Although the variations of thickness and refractive index versus time (data not shown) share a similar form for FN on both $(PAH-PSS)_4-PAH$ and $(PAH-PSS)_5$ films, we note the FN layer thickness on the $(PAH-PSS)_4-PAH$ film to be almost double that on the $(PAH-PSS)_5$ film and the overall film (PEM + FN) refractive index to be generally higher in the latter case. The steady increase (decrease) in thickness (refractive index) during FN adsorption indicates a FN layer initially composed of molecules with significant surface contact and later by more and more molecules extending away from the surface into solution. The characteristic parameters of the FN layers on $(PAH-PSS)_4-PAH$ and $(PAH-PSS)_5$ are shown in Table 1.

To analyze the influence of the ionic strength on FN adsorption onto the PEM films, we repeat the above experiments with a buffer containing a higher salt concentration ([NaCl] = 1.0 M). We find (Table 1) the higher ionic strength buffer to lead to PEM films of greater thickness (by roughly a factor of 2) and to FN layers of lesser thickness (by roughly a factor of 4). However, the thickness of FN on $(PAH-PSS)_4-PAH$ remains about double that on $(PAH-PSS)_5$.

Monoclonal IgG (AntiFN) Adsorption. One of our goals is to demonstrate the possibility of influencing protein orientation and conformation through PEM film properties. Although the previously mentioned results suggest such an influence, to further investigate this effect, we consider here the binding to adsorbed FN layers of monoclonal antibodies specific to an epitope at the protein's cell binding site. This provides direct information on binding-site accessibility and is an indirect measure of FN orientation and conformation.

We consider FN layers on $(PAH-PSS)_4-PAH$ and $(PAH-PSS)_5$ PEM films formed from bulk protein concentrations of 2 and 50 μg/mL and HEPES buffers of [NaCl] = 0.1 M. The densities of these FN layers are respectively 0.7 and 1.14 μg/cm^2 on the positively charged $(PAH-PSS)_4-PAH$ film and 0.18 and 0.51 μg/cm^2 respectively on the negatively charged $(PAH-PSS)_5$ film. In Figure 4A, we show FN adsorption kinetics (at a concentration of 50 μg/mL) onto the PEM films and those of AntiFN onto the FN layer. In Figure 4b, we compare the kinetics of adsorption of AntiFN to those of AntiCC (anti-cytochrome c) onto identically prepared PEM + FN layers. AntiCC is virtually identical structurally to AntiFN, but binds specifically only to the protein cytochrome c and so should have no specificity toward FN. Any binding of AntiFN in excess of that of AntiCC can, therefore, be attributed to specific binding at the cell binding site. The initial kinetics of AntiFN and AntiCC adsorption are identical, suggesting initial attachment to be nonspecific. [Nonspecific binding of (positively charged) IgG may result from interactions with PSS molecules within the PEM film.] However, the

(49) Ramsden, J. J.; Lvov, Y. M.; Decher, G. *Thin Solid Films* **1995**, *254*, 246−251.
(50) Ramsden, J. J.; Lvov, Y. M.; Decher, G. *Thin Solid Films* **1995**, *261*, 343−344.

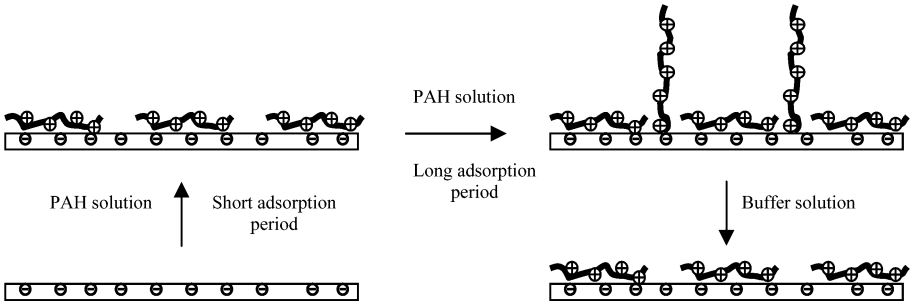

Figure 2. Schematic of the PAH film structure. Initial adsorption is quite flat, owing to strong electrostatic attraction. Subsequent adsorption involves considerable polyelectrolyte extension away from the surface. These more extended molecules desorb during rinsing.

Table 1. Thickness, Refractive Index, and Density of PEM Films and FN Adsorbed to PEM Films, from HEPES Buffer of pH 7.4 and of [NaCl] = 1.0 and 0.1 M, As Determined from OWLS[a]

		[NaCl] = 0.1 M			[NaCl] = 1.0 M		
adsorbed layer	surface charges	thickness (nm)	density (μg cm^{-2})	refractive index	thickness (nm)	density (μg cm^{-2})	refractive index
$(PAH-PSS)_4-PAH$	+	14.1 ± 0.4	1.01 ± 0.02	1.486 ± 0.007	25.4 ± 0.1	2.03 ± 0.15	1.499 ± 0.011
FN		19.6 ± 0.7	1.14 ± 0.09		4.5 ± 0.3	0.282 ± 0.007	
$(PAH-PSS)5$	−	16.3 ± 0.4	1.27 ± 0.06	1.487 ± 0.011	33.1 ± 0.6	2.45 ± 0.11	1.487 ± 0.004
FN		9.9 ± 1.0	0.51 ± 0.03		2.7 ± 0.3	0.167 ± 0.004	

[a] Each value is taken following a buffer rinse, as shown in Figures 1 and 3, and is the mean of three experiments. The uncertainty is the standard deviation of this mean value.

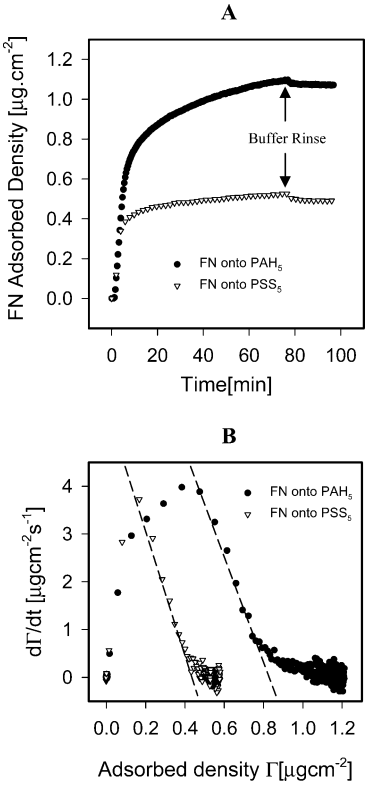

Figure 3. (A) Adsorbed density versus time and (B) the adsorption rate versus adsorbed amount for FN, at a concentration of 50 μg/mL in HEPES buffer of [NaCl] = 0.1 M, onto (positively charged) $(PAH-PSS)_4-PAH$ (●) and (negatively charged) $(PAH-PSS)_5$ (▽) films. Arrows show the onset of a buffer rinse.

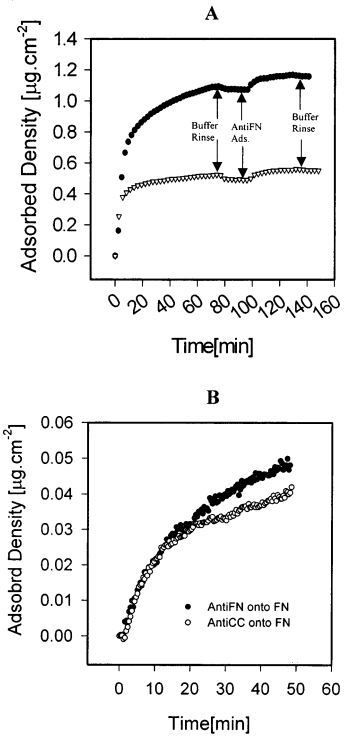

Figure 4. (A) Adsorbed density versus time of FN and, subsequently, AntiFN (monoclonal IgG of concentration 0.5 μg/mL in HEPES buffer of [NaCl] = 0.1 M) adsorbed onto $(PAH-PSS)_4-PAH$ (●) or $(PAH-PSS)_5$ (▽) films. Intervening buffer rinses are shown as well. (B) The adsorbed density versus time of AntiFN and AntiCC onto FN adsorbed layers on $(PAH-PSS)_5$ films.

curves begin to systematically deviate at about 1200 s as a result, we believe, of specific binding of the AntiFN. (A repeat experiment showed similar behavior.) In Table 2, we summarize data from the AntiFN and AntiCC binding experiments. We observe the ratios of AntiFN to FN on the $(PAH-PSS)_4-PAH$ film to be identical (0.29) for FN layers formed at either concentration. On the $(PAH-PSS)_5$ film, the ratios are 0.55 and 0.46 for FN layers formed at 2 and 50 μg/mL, respectively. Binding to the lower-concentration FN layer of AntiCC was significantly lower (an AntiFN/FN binding ratio of 0.41). We, therefore, conclude that the cell binding sites of FN on the PSS-terminated film are significantly more accessible than those on the PAH-terminated film.

Table 2. Density and Thickness of FN and Subsequent AntiFN or AntiCC Adsorbed to PEM Films[a]

	FN			IgG (AntiFN) onto FN; adsorption time = 30 min	
PEM terminal layer	bulk concentration (μg mL^{-1})	density (μg cm^{-2})	thickness (nm)	ads. density (μg cm^{-2})	$(\Gamma_{IgG}/m_{IgG})/(\Gamma_{FN}/m_{FN})$
PAH	2	0.7	10.6	0.0546	0.29
	50	1.14	19.6	0.0906	0.29
PSS	2	0.28	5.1	0.0394	0.55
	50	0.51	9.9	0.0643	0.46

				IgG (AntiCC) onto FN; adsorption time = 30 min	
PEM terminal layer	bulk concentration (μg mL^{-1})	density (μg cm^{-2})	thickness (nm)	ads. density (μg cm^{-2})	$(\Gamma_{IgG}/m_{IgG})/(\Gamma_{FN}/m_{FN})$
PSS	2	0.29	5.01	0.0326	0.41

[a] AntiFN is a monoclonal antibody (IgG) specific to an epitope located at the cell binding site of FN, and AntiCC is a monoclonal antibody to cytochrome c (and, thus, not specific to any region of FN). Each value is taken following a buffer rinse, as shown in Figures 1 and 3. Also shown is the molar ratio of antibody to FN.

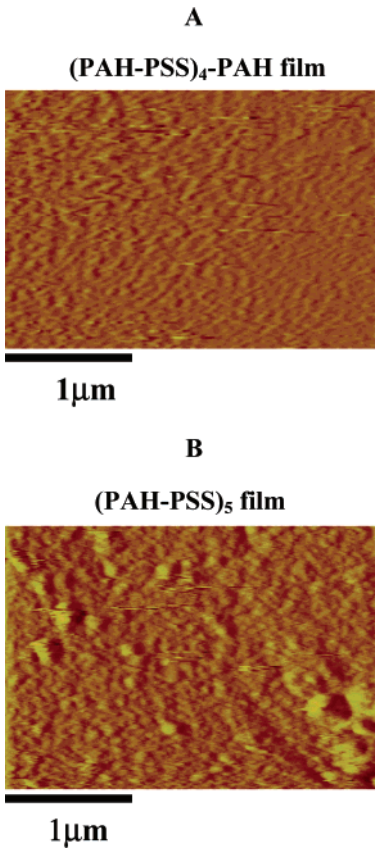

Figure 5. Contact-mode AFM height images of (A) $(PAH-PSS)_4-PAH$ and (B) $(PAH-PSS)_5$ films.

AFM Analysis. We employ contact-mode AFM to investigate the topography of the PEM films and FN layers adsorbed to these films. In Figure 5, we show AFM images of the $(PAH-PSS)_4-PAH$ and $(PAH-PSS)_5$ PEM films. In the case of a PAH terminal layer, the adsorbing surface is quite smooth. The root-mean-square roughness, as determined by the roughness analysis (data not shown), is approximately 3.3 nm, a value close to the thickness of an adsorbed polyelectrolyte bilayer. When PSS is the terminal layer, the adsorbing surface is significantly rougher (around 6.5 nm) and some aggregates appear on the surface. These possibly form as a result of the relatively hydrophobic styrene groups of PSS. Despite the presence of clusters, the PSS surface remains sufficiently smooth to ultimately distinguish larger particles as they subsequently attach.

In Figure 6, we show AFM images and cross-section analyses of FN adsorbed to the PEM films. We observe FN adsorption on a PAH-terminated film to result in (relatively few) polydisperse aggregates of broad size and shape distributions and that on PSS terminated films to result in (numerous) aggregates of narrow size and shape distributions. The length and width of aggregates on PAH are measured to be 280 ± 80 nm and 150 ± 50 nm, respectively, whereas on PSS, these values are respectively 150 ± 20 nm and 120 ± 20 nm. From the cross-section analyses, the estimated heights of the FN clusters on PAH and PSS are respectively 36 ± 16 nm and 25 ± 10 nm. Taking 1.0 g/cm^3 as the density of a single FN molecule (a lower-bound estimate) and using the software package "ImageJ" (available free from the National Science Foundation web page) to determine the area covered by the clusters, we estimate the contribution to the FN density from the clusters to be 0.13 and 0.23 μg/cm^2 (or 11 and 45% of the total FN density) for the PAH- and PSS-terminated films, respectively. The high protein density measured by OWLS on the PAH terminated film, together with the fairly smooth section analysis baseline, suggest that a relatively smooth and confluent FN monolayer exists along with the aggregates and that the measured cluster height is relative to this monolayer. The higher fraction of protein within clusters and the somewhat lower protein density on the PSS-terminated film indicate that the measured cluster height is likely relative to the underlying PEM film.

In both cases, the AFM-determined cluster heights are greater than the OWLS-determined FN layer thicknesses. As a result of the sparse nature of the aggregates on the PAH-terminated film, we believe the measured OWLS thickness (19.6 ± 0.7 nm) corresponds to the dense FN monolayer, that is, it is not significantly affected by the aggregates. In contrast, the dense aggregates observed on the PSS-terminated film most likely do affect the measured thickness; in this case, we believe the OWLS thickness (9.9 ± 1.0 nm) represents an average of the aggregates and the space between aggregates. We note that aggregation occurs following adsorption (aggregates in the bulk are removed prior to adsorption studies via filtration), a phenomenon not uncommon in adsorbed FN systems.[40,51,52]

(51) Calonder, C.; Tie, Y.; Van Tassel, P. R. *Proc. Natl. Acad. Sci. U.S.A.* **2001**, *98*, 10664−10669.
(52) Tie, Y.; Calonder, C.; Van Tassel, P. R. *J. Colloid Interface Sci.* **2003**, *268*, 1−11.

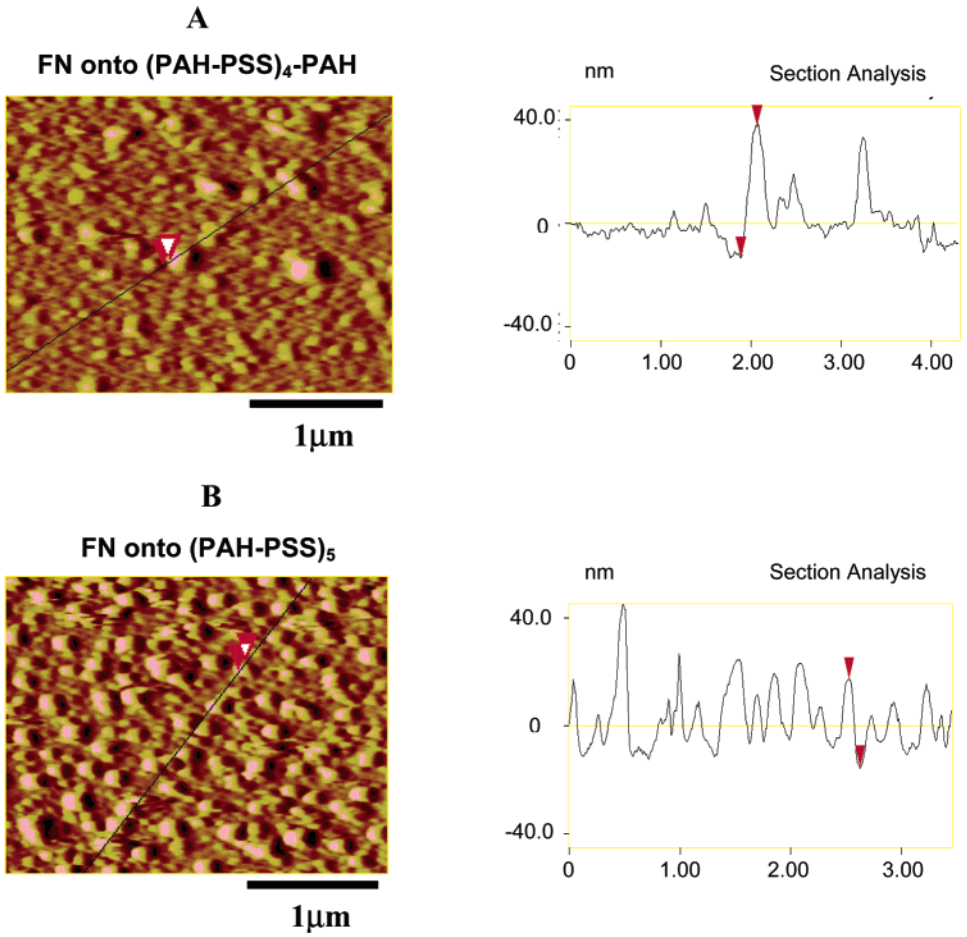

Figure 6. Contact-mode AFM height images and corresponding section analyses of FN adsorbed onto (A) $(PAH-PSS)_4-PAH$ and (B) $(PAH-PSS)_5$ films.

Discussion

Controlling adsorbed protein layer structure is important for tissue engineering and biosensing applications. Among the many proteins of biological significance, FN is particularly interesting owing to its established effect on living cells. However, most previous studies employing FN focus primarily on the biological activity, not the structure, of the adsorbed layer. In principle, controlling the adlayer structure would allow one to modulate biological activity in a targeted way. Here, we investigate the control of adsorbed FN via an underlying PEM film formed by the alternate deposition of polyanionic and polycationic species. By choice of solution pH, ionic strength, and terminal film layer, one has considerable control over the protein−substrate interactions ultimately directing adlayer structure. We demonstrate here the significant influence of the terminal PEM film layer: a FN layer adsorbed to $(PAH-PSS)_4-PAH$ is considerably denser, thicker, less prone to clustering, and less prone to binding monoclonal antibodies than a FN layer adsorbed to $(PAH-PSS)_5$.

PEM films composed of the polyelectrolytes PAH and PSS have been the subject of several previous investigations.[47,49,50,53−58] In particular, Ladam et al.[47] have shown the PEM thickness to grow linearly with layer number for layers added beyond an initial "precursor zone" of 5−6 layers. We observe the onset of linear growth to occur at an even smaller layer number; in this sense, our films do not exhibit an obvious precursor zone. Although buffer (Tris versus HEPES), adsorbing surface (silica versus STO), and precursor layer (polyethylene imine versus none) differ between their work and our own, owing to the nearly identical pH and ionic strength of these buffers, we believe the differences between the surfaces to be at the origin of the discrepant behavior. Precursor zone thickness likely depends on substrate properties such as surface chemistry, charge, roughness, and so forth as well as on film growth conditions such as pH, ionic strength, and polyelectrolyte concentration. It appears that the subtle property differences between silica and STO cause this rather large change in precursor zone extent. The "linear zone" may also exhibit a strong dependence on the underlying substrate. We find the incremental layer thickness on STO to be almost twice as large as that on an indium tin oxide adsorbing surface (data not shown). The substrate sensitivity observed here points toward a need to systematically characterize the substrates underlying PEM films to ensure reproducibility.

We observe FN to interact strongly with both positively and negatively charged PEM films. This is consistent with earlier reports for other proteins.[18] Previous studies of FN adsorption to bare substrates[40,51] (i.e., without a PEM

(53) Decher, G.; Hong, J. D.; Schmitt, J. *Thin Solid Films* **1992**, *210*, 831−835.
(54) Lvov, Y.; Haas, H.; Decher, G.; Mohwald, H.; Kalachev, A. *J. Phys. Chem.* **1993**, *97*, 12835−12841.
(55) Schmitt, J.; Grunewald, T.; Decher, G.; Pershan, P. S.; Kjaer, K.; Losche, M. *Macromolecules* **1993**, *26*, 7058−7063.
(56) Caruso, F.; Niikura, K.; Furlong, D. N.; Okahata, Y. *Langmuir* **1997**, *13*, 3422−3426.
(57) Chen, W.; McCarthy, T. J. *Macromolecules* **1997**, *30*, 78−86.
(58) Losche, M.; Schmitt, J.; Decher, G.; Bouwman, W. G.; Kjaer, K. *Macromolecules* **1998**, *31*, 8893−8906.

film) show adsorbed amounts at saturation to be about 5 and 2.5 times smaller respectively than those onto the positively and negatively charged PEM films studies here. Dense FN layers such as those occurring on PEM films may be significant in terms of enhanced biological activity. We speculate further in the following on the underlying causes of PEM enhancement to FN adsorption.

AFM images reveal FN clustering on PEM films. While aggregation could indeed lead to protein layers of high density, this explanation is probably not sufficient because Guemouri et al.[40] and Calonder et al. [51] have also observed significant surface clustering of FN on bare STO substrates with far lower overall protein layer densities. These results, from studies employing buffers near physiological ionic strength (0.1−0.2 M), are not unexpected because under these conditions, FN possesses a compact conformation whose physiological function is to aggregate at interfaces.[59,60] The important question here concerns the specific role of the PEM film in FN clustering. In one extreme, the PEM may act as a more or less rigid substrate on which FN diffuses, changes conformation, and ultimately forms clusters. However, it is likely that the PEM film is quite flexible and that polyelectrolyte molecules may themselves diffuse and partially cover the adsorbed FN molecules. This would act to increase the electrostatic attraction between "coated" FN molecules with those previously adsorbed as well as those arriving from the bulk. Ladam et al.[18] first introduced this idea within the framework of albumin adsorption onto PEM films. Although protein aggregation on PEM films is observed here and elsewhere,[18] PEM films have also been reported to actually suppress aggregation.[23,30]

To better characterize the interactions occurring in the PEM + FN films, we propose the following kinetic analysis. As shown previously, beyond the transport-limited regime, the adsorption rate can be used to characterize protein−surface and protein−protein interactions.[52] An equation relating the rate of adsorption to the adsorbed layer structure is as follows:[52]

$$d\Gamma/dt = k_a c_b \Phi - \sum_i k_{d,i}\Gamma_i \qquad (3)$$

where k_a is the adsorption rate constant, c_b is the bulk protein concentration, Φ is the one-body cavity function (a measure of the probability of a cavity on the surface free from adsorbed protein), $k_{d,i}$ is the desorption rate constant for an adsorbed protein in state i, and Γ_i is the density of adsorbed protein in state i. Because Φ and the Γ_i's are analytic functions of the density and, thus, expandable as Taylor series, a plot of $d\Gamma/dt$ versus Γ should then yield a linear region whose intercept is $k_a c_b \Phi(\Gamma = 0) = k_a' c_b$ (where k_a' is the apparent adsorption rate constant) and whose slope is $k_a c_b A_1 - \bar{k}_d$ (where A_1 is the linear coefficient to the Φ expansion and $\bar{k}_d$ is an average desorption rate weighted by the lowest-order terms in the Γ_i expansions). In Figure 3B, we show such plots for FN adsorption onto $(PAH-PSS)_4-PAH$ and $(PAH-PSS)_5$ PEM films. The dashed lines are least-squares fits to the linear parts of these curves; their intercepts yield k_a' values of $(2.04 \pm 0.08) \times 10^{-4}$ cm/s and $(1.20 \pm 0.02) \times 10^{-4}$ cm/s on PAH- and PSS-terminated PEM films, respectively. From these values, we conclude the FN adsorption energy barrier to be higher on $(PAH-PSS)_5$ than on $(PAH-PSS)_4-PAH$. Both of these k_a' values are considerably greater than those reported for adsorption onto bare STO (from 0.4×10^{-4} to 0.8×10^{-4} cm/s).[51,52]

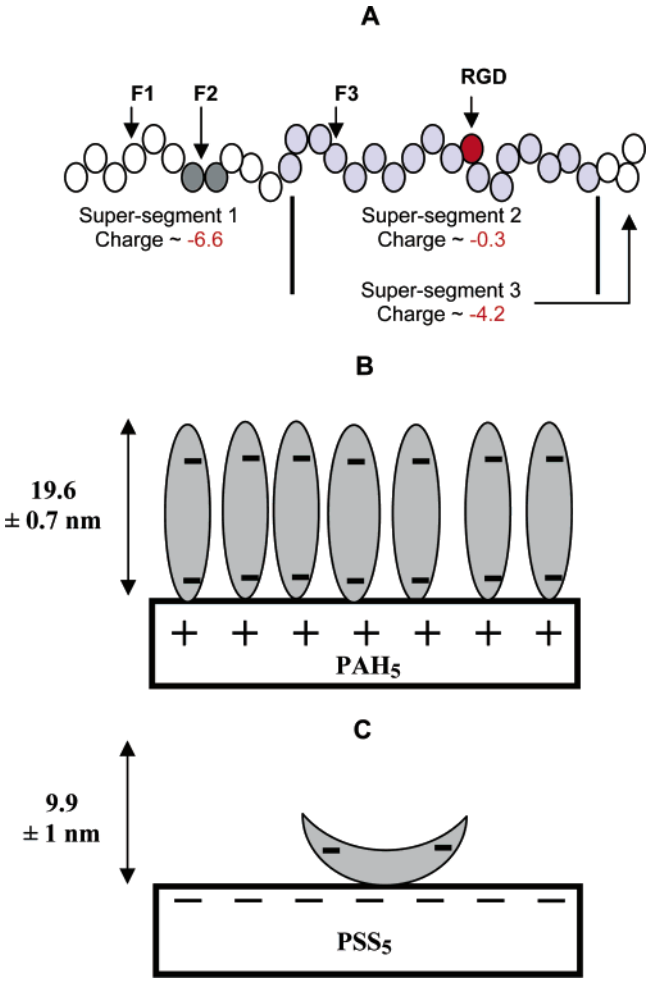

Figure 7. (A) Schematic of the modular FN molecule with charge distribution based on constituent amino acids at pH = 7.4. Three adjacent supersegments are identified carrying approximate charges of −6.6, −0.3, and −4.2. (B) A schematic of FN adsorbing in an end-on orientation on a positively charged $(PAH-PSS)_4-PAH$ film. The OWLS-measured thickness is thought to correspond to the height on this monolayer. (C) A schematic of an individual FN adsorbing in a side-on orientation on a negatively charged $(PAH-PSS)_5$ film. The V-like conformation results from repulsion between the end segments and the surface. The OWLS-measured thickness is somewhat greater than the height of this molecule; it is thought to correspond to an average height of clusters plus regions outside of the clusters.

FN is a highly flexible glycoprotein composed of two nearly identical covalently linked subunits. Each FN chain consists of quasi-independent domains characterized by various amino acid repeat sequences.[60] On the basis of the known charges of the constituent amino acids at the buffer pH, one may think of the modular FN as being composed of three adjacent supersegments carrying approximate charges −6.6, −0.3, and −4.2 (see Figure 7A). The end segments, thus, carry strong negative charges whereas the middle segment is almost neutral. One could, therefore, suppose that, on a positively charged surface, FN would adsorb in an end-on orientation and a nearly linear (vertical) conformation (Figure 7B). MacDonald et al. have reported FN dimensions of 16.6 nm × 9.6 nm × 2.5 nm;[61] these are consistent with the picture of Figure

(59) Rocco, M.; Carson, M.; Hantgan, R.; McDonagh, J.; Hermans, J. *J. Biol. Chem.* **1983**, *258*, 4545−4549.
(60) Rocco, M.; Infusini, E.; Daga, M. G.; Gogioso, L.; Cuniberti, C. *EMBO J.* **1987**, *6*, 2343−2349.
(61) MacDonald, D. E.; Markovic, B.; Allen, M.; Somasundaran, P.; Boskey, A. L. *J. Biomed. Mater. Res.* **1998**, *41*, 120−130.

7B taken together with our OWLS layer thickness data (Table 1). The enhanced binding of AntiFN on the PSS-terminated surface suggests a more exposed central region of FN. Because clustered FN molecules would not likely bind to antibodies, this suggests FN molecules not contained in clusters to exist in a horizontal orientation, as shown in Figure 7C.

Finally, we add a few words on the analysis of OWLS data. By using eq 1, we invoke the assumption of a single optically uniform adsorbed layer, even for the case of protein adsorbing to a PEM film. Picart et al. have tested this assumption by analyzing protein−PEM films via both one and two layer models. They found the resulting adsorbed layer density to differ by about 2% and the adsorbed layer thickness to differ by about 10% (these differences were somewhat greater when the protein layers were considerably thinner than those reported here). Because these numbers are of the same order as the experimental uncertainty, we feel the single-layer model is justified. It should also be mentioned that the derivation of eq 1 involves a first-order expansion of reflection coefficients in $k_0 t_A$, where $k_0 = 2\pi/\lambda$.[44] For the thickest films presented here, $k_0 t_A$ is about 0.4. Although the limit of validity of this expansion has not been directly tested for OWLS, Heinrich et al. recently showed the expansion to be valid up to $k_0 t_A = 0.5$ in the context of scanning angle reflectometry.[62] Owing to the similarity of these two methods, we feel the linear expansion is justified for the adsorbed layers considered here.

Conclusions

We present here a study of FN adsorption to the surface of PEM films composed of alternating layers of PAH and PSS. While adsorption in all cases exceeds that observed onto standard flat metal oxide surfaces, the density and thickness of FN on a (positively charged) PAH-terminated film are roughly double those on a (negatively charged) PSS-terminated film. With increased salt, the PEM film grows thicker but the FN layer becomes thinner. We observe significant clustering on the negatively charged film. By additionally considering the extent to which monoclonal antibodies bind to adsorbed FN, we propose an adsorbed layer with an end-on (side-on) orientation on the PAH-(PSS-)terminated film. The significant influence of both the film terminal layer and the salt concentration bodes well for applications demanding protein adlayer structural control.

Acknowledgment. We thank Pierre Schaaf and Jean-Claude Voegel for helpful discussions and the National Science Foundation (CTS-9733310) and the National Institutes of Health (R01-EB00258) for financial support.

LA035479Y

(62) Heinrich, L.; Mann, E. K.; Voegel, J. C.; Schaaf, P. *Langmuir* **1997**, *13*, 3177−3186.